INTERNATIONAL JOURNAL FOR NUMERICAL METHODS IN FLUIDS
Int. J. Numer. Meth. Fluids 2010; **62**:747–764
Published online 20 March 2009 in Wiley InterScience (www.interscience.wiley.com). DOI: 10.1002/fld.2041

A compact finite difference method for solving Burgers' equation

Shusen Xie[1,*,†], Guangxing Li[1], Sucheol Yi[2] and Sunyeong Heo[3]

[1]*School of Mathematical Sciences, Ocean University of China, Qingdao 266071, People's Republic of China*
[2]*Department of Applied Mathematics, Changwon National University, Changwon 641-773, Republic of Korea*
[3]*Department of Statistics, Changwon National University, Changwon 641-773, Republic of Korea*

SUMMARY

In this paper, a high-order accurate compact finite difference method using the Hopf–Cole transformation is introduced for solving one-dimensional Burgers' equation numerically. The stability and convergence analyses for the proposed method are given, and this method is shown to be unconditionally stable. To demonstrate efficiency, numerical results obtained by the proposed scheme are compared with the exact solutions and the results obtained by some other methods. The proposed method is second- and fourth-order accurate in time and space, respectively. Copyright © 2009 John Wiley & Sons, Ltd.

Received 20 August 2008; Revised 15 December 2008; Accepted 10 February 2009

KEY WORDS: Burgers' equation; Hopf–Cole transformation; compact difference scheme; convergence; stability

1. INTRODUCTION

Consider the one-dimensional nonlinear Burgers' equation

$$u_t + uu_x = vu_{xx}, \quad a<x<b, \ \ 0<t\leqslant T \tag{1}$$

with the initial condition

$$u(x,0) = f(x), \quad a<x<b \tag{2}$$

and boundary conditions

$$u(a,t) = u(b,t) = 0, \quad 0<t\leqslant T \tag{3}$$

*Correspondence to: Shusen Xie, School of Mathematical Sciences, Ocean University of China, Qingdao 266071, People's Republic of China.
†E-mail: shusenxie@ouc.edu.cn

Contract/grant sponsor: NNSF; contract/grant number: 40276008
Contract/grant sponsor: Changwon National University

where $v>0$ is the coefficient of kinematic viscosity, f is a prescribed function, and the subscripts t and x denote differentiation with respect to variables t and x, respectively. Equation (1) was first introduced by Bateman [1] and later treated by Burgers [2] after whom such an equation is widely referred to as Burgers' equation. This equation plays a major role in the study of nonlinear waves since it is used as a mathematical model in turbulence problems, in the theory of shock waves, and in continuous stochastic processes [3]. Many scientists are devoted to studying the exact and numerical solution of the Burgers equation. The Burgers equation (1) is one of the very few nonlinear partial differential equation that can be solved analytically for limited set of initial condition functions only. Benton and Platzman [4] surveyed exact solutions of one-dimensional Burgers' equations and have given many different analytic solutions for the Burgers equation with distinct initial conditions. In many cases these solutions involve infinite series, which may converge very slowly for small values of $v>0$ (cf. [5]). Many researchers have used various numerical techniques to solve the equation numerically such as the finite difference, the finite element, the boundary element, and the spectral methods. See [6–15] and literatures are therein.

Kutluay *et al.* [6] introduced the explicit finite difference and exact explicit finite difference methods to solve the linearized heat equation with Neumann boundary conditions obtained by applying the Hopf–Cole transformation to the Burgers equation. Kadalbajoo and Awasthi [7] have applied the Crank–Nicolson method to the linearized equation and shown that the method based on the Crank–Nicolson method is unconditionally stable. The accuracy of this method is second-order accurate both in space and time.

In this paper, we derive a high-order accurate compact finite difference method (FDM) to numerically solve the linearized equation. The present method gives an implicit scheme with tridiagonal symmetric positive-definite system, which can be easily implemented. Stability and convergence analyses show that the present method is unconditionally stable and has an accuracy of second- and fourth-order in time and space, respectively. Numerical experiments show that the accuracy of the present method and the fourth-order iterative FDM provided in [8] is almost the same. The numerical solutions obtained by the present method are in good agreement with the exact solutions, and our method gives compatible numerical results with the ones obtained by some other available methods given in references.

In Section 2 we consider a fourth-order accurate FDM using the Hopf–Cole transformation. The stability and convergence analyses of the proposed scheme are given in Section 3, and the results of numerical experiment are shown in Section 4.

2. FOURTH-ORDER ACCURATE COMPACT FINITE DIFFERENCE SCHEME

By substituting the Hopf–Cole transformation

$$u(x,t)=-2v\frac{\theta_x}{\theta} \tag{4}$$

into the Burgers equation (1), we can obtain the linearized equation

$$\theta_t=v\theta_{xx} \tag{5}$$

One can see that the Hopf–Cole transformation (4) is a solution to (1) for any function θ satisfying (5). Therefore, the initial and boundary value problem of Burgers' equation can be

DOI: 10.1002/fld

reduced to the following linearized equation with the initial and homogeneous Neumann boundary conditions:

$$\begin{aligned} \theta_t &= v\theta_{xx}, \quad a<x<b, \ \ 0<t\leqslant T \\ \theta(x,0) &= \varphi(x) = \exp\left(-\frac{1}{2v}\int_a^x f(s)\,\mathrm{d}s\right), \quad a<x<b \\ \theta_x(a,t) &= \theta_x(b,t) = 0, \quad 0<t\leqslant T \end{aligned} \tag{6}$$

The solution domain $\Omega=\{(x,t)\,|\,a\leqslant x\leqslant b, 0\leqslant t\leqslant T\}$ is discretized into grids described by the set $\{(x_i,t_k)\}$ of nodes, in which $x_i=a+ih, i=0,1,\ldots,J$, and $t_k=k\tau, k=0,1,\ldots,N=T/\tau$, where h and τ are mesh sizes for space and time variables, respectively.

Let $v_i^k=v(x_i,t_k)$. We use the following notations for simplicity:

$$v_i^{k+1/2} := \frac{1}{2}(v_i^{k+1}+v_i^k), \quad \partial_t v_i^{k+1} := \frac{1}{\tau}(v_i^{k+1}-v_i^k)$$

$$D_x v_i^k := \frac{1}{h}(v_{i+1}^k - v_i^k), \quad D_{\hat{x}} v_i^k := \frac{1}{2h}(v_{i+1}^k - v_{i-1}^k)$$

$$\delta_x^2 v_i^k := \frac{1}{h}(D_x v_i^k - D_x v_{i-1}^k) = \frac{1}{h^2}(v_{i+1}^k - 2v_i^k + v_{i-1}^k)$$

By setting $w=v\theta_{xx}$, the Equation (5) can be written as $w=\theta_t$. Assume that the solution θ is sufficiently smooth. By the Taylor expansion, we get

$$w_i^{k+1/2} = \partial_t \theta_i^{k+1} + O(\tau^2) \tag{7}$$

and

$$\begin{aligned} w_i^{k+1/2} &= v(\theta_{xx})_i^{k+1/2} = v\delta_x^2\theta_i^{k+1/2} - v\frac{h^2}{12}(\theta_{xxxx})_i^{k+1/2} + O(h^4) \\ &= v\delta_x^2\theta_i^{k+1/2} - \frac{h^2}{12}(w_{xx})_i^{k+1/2} + O(h^4) \\ &= v\delta_x^2\theta_i^{k+1/2} - \frac{h^2}{12}\delta_x^2 w_i^{k+1/2} + O(h^4) \end{aligned} \tag{8}$$

Substituting (7) into (8), we obtain

$$\tfrac{1}{12}(\partial_t\theta_{i-1}^{k+1} + 10\partial_t\theta_i^{k+1} + \partial_t\theta_{i+1}^{k+1}) - v\delta_x^2\theta_i^{k+1/2} = O(\tau^2+h^4) \tag{9}$$

Let Θ_i^k denote the approximation of θ_i^k. From (9) we obtain the following compact finite difference scheme to solve problem (6):

$$\begin{aligned} \tfrac{1}{12}(\partial_t\Theta_{i-1}^{k+1} + 10\partial_t\Theta_i^{k+1} + \partial_t\Theta_{i+1}^{k+1}) - v\delta_x^2\Theta_i^{k+1/2} = 0, \quad 0\leqslant i\leqslant J \\ D_{\hat{x}}\Theta_0^{k+1} = D_{\hat{x}}\Theta_J^{k+1} = 0 \\ \Theta_i^0 = \varphi(x_i) \end{aligned} \tag{10}$$

DOI: 10.1002/fld

By the approximation of boundary conditions in (10), this scheme can be written as

$$\tfrac{1}{12}(\partial_t\Theta_{i-1}^{k+1}+10\partial_t\Theta_i^{k+1}+\partial_t\Theta_{i+1}^{k+1})-v\delta_x^2\Theta_i^{k+1/2}=0,\quad 1\leqslant i\leqslant J-1$$

$$5\partial_t\Theta_0^{k+1}+\partial_t\Theta_1^{k+1}-\frac{12v}{h}D_x\Theta_0^{k+1/2}=0$$

$$\partial_t\Theta_{J-1}^{k+1}+5\partial_t\Theta_J^{k+1}+\frac{12v}{h}D_x\Theta_{J-1}^{k+1/2}=0,\quad 0\leqslant k\leqslant N-1$$

$$\Theta_i^0=\varphi(x_i)$$

The above scheme can be rewritten as the following matrix equation:

$$(A+vrB)\boldsymbol{\Theta}^{k+1}=(A-vrB)\boldsymbol{\Theta}^k,\quad k=0,1,\ldots,N-1 \tag{11}$$

where $\boldsymbol{\Theta}^k=(\Theta_0^k,\Theta_1^k,\ldots,\Theta_J^k)^{\mathrm{T}}$, $r=\tau/h^2$, and

$$A=\begin{pmatrix}5&1&0&\cdots&0\\1&10&1&\ddots&\vdots\\0&\ddots&\ddots&\ddots&0\\\vdots&\ddots&1&10&1\\0&\cdots&0&1&5\end{pmatrix},\quad B=\begin{pmatrix}6&-6&0&\cdots&0\\-6&12&-6&\ddots&\vdots\\0&\ddots&\ddots&\ddots&0\\\vdots&\ddots&-6&12&-6\\0&\ldots&0&-6&6\end{pmatrix}$$

Since the matrix $A+vrB$ is symmetric tridiagonal and strictly diagonally dominant, Equation (11) has a unique solution and can be easily solved. From (9) we know that this scheme has a truncation error of order $O(\tau^2+h^4)$ for $i=1,\ldots,J-1$.

Integrating (4) with respect to variable x on the interval $[x_{i-1},\ x_{i+1}]$ for $i=1,\ldots,J-1$, we have

$$\int_{x_{i-1}}^{x_{i+1}}u(x,t_k)\,\mathrm{d}x=-2v\int_{x_{i-1}}^{x_{i+1}}\frac{\theta_x(x,t_k)}{\theta(x,t_k)}\,\mathrm{d}x=-2v\ln\left|\frac{\theta(x_{i+1},t_k)}{\theta(x_{i-1},t_k)}\right|$$

By applying Simpson's rule for the integration in the above equation, we obtain

$$u_{i-1}^k+4u_i^k+u_{i+1}^k=-\frac{6v}{h}\ln\left|\frac{\theta_{i+1}^k}{\theta_{i-1}^k}\right|+O(h^4)$$

Let U_i^k denote the approximation of u_i^k. Then we get the linear algebraic system

$$U_{i-1}^k+4U_i^k+U_{i+1}^k=F_i^k,\quad 1\leqslant i\leqslant J-1 \tag{12}$$

where

$$F_i^k=-\frac{6v}{h}\ln\left|\frac{\Theta_{i+1}^k}{\Theta_{i-1}^k}\right|$$

DOI: 10.1002/fld

Since $U_0^k = U_J^k = 0$, the Equation (12) can be written as

$$\begin{pmatrix} 4 & 1 & 0 & \cdots & 0 \\ 1 & 4 & 1 & \ddots & \vdots \\ 0 & \ddots & \ddots & \ddots & 0 \\ \vdots & \ddots & 1 & 4 & 1 \\ 0 & \dots & 0 & 1 & 4 \end{pmatrix} \begin{pmatrix} U_1^k \\ U_2^k \\ \vdots \\ \vdots \\ U_{J-1}^k \end{pmatrix} = \begin{pmatrix} F_1^k \\ F_2^k \\ \vdots \\ \vdots \\ F_{J-1}^k \end{pmatrix}$$

The coefficient matrix in the above equation is tridiagonal symmetric positive definite, and the above linear system is well-conditioned, since the eigenvalues of the matrix are $\lambda_i = 4 + 2\cos(i\pi/J)$ for $i = 1, 2, \dots, J-1$ and, hence, the spectral condition number is less than 3, where the spectral condition number is defined as the ratio of the largest and smallest eigenvalues. This linear matrix equation can be easily solved by using direct or iterative methods.

3. STABILITY AND CONVERGENCE ANALYSES

In this section we investigate the stability and convergence rate of the present scheme by the energy method. Let $I_h = \{x_0, \dots, x_J\}$ denote the set of nodes of the interval $I = [a, b]$. For any grid functions f and g defined on I_h, we define the following discrete L_2-inner products:

$$\langle f,\ g\rangle = \frac{h}{2}(f_0 g_0 + f_J g_J) + \sum_{i=1}^{J-1} f_i g_i h \tag{13}$$

$$\langle f,\ g\rangle_l = \sum_{i=0}^{J-1} f_i g_i h \tag{14}$$

and the respective associated norms are defined by

$$\|f\|_{L_2} = \sqrt{\langle f,\ f\rangle}, \quad |\|f|\|_{L_2} = \sqrt{\langle f,\ f\rangle_l} \tag{15}$$

We also use the following discrete norms in this section:

$$\|f\|_{L_\infty} = \max_{0 \leqslant i \leqslant J} |f_i|, \quad \|f\|_{H^1}^2 = \|f\|_{L_2}^2 + |\|D_x f|\|_{L_2}^2 \tag{16}$$

The following lemmas can be proved without difficulty.

Lemma 1
For any grid functions f and g defined on $\widetilde{I}_h = \{x_{-1}, x_0, \dots, x_{J+1}\}$, we have

$$\langle \delta_x^2 f, g\rangle = -\langle D_x f, D_x g\rangle_l - (D_{\hat{x}} f_0) g_0 + (D_{\hat{x}} f_J) g_J \tag{17}$$

Lemma 2
For any grid function f defined on I_h, we have the inequality

$$|\|D_x f|\|_{L_2}^2 \leqslant \frac{4}{h^2}\|f\|_{L_2}^2 \tag{18}$$

DOI: 10.1002/fld

Lemma 3
For any grid function f defined on I_h, we have the inequality

$$\|f\|_{L_\infty} \leqslant M_0 \|f\|_{H^1} \tag{19}$$

where $M_0 = \max\{1/\sqrt{b-a},\ \sqrt{b-a}\}$.

Theorem 4
Let Θ_i^n be the solution of scheme (10). Then we have

$$\|\Theta^n\|_{L_2}^2 \leqslant \tfrac{3}{2}\|\Theta^0\|_{L_2}^2, \quad 1 \leqslant n \leqslant N \tag{20}$$

Proof
By taking the inner product $\langle \cdot, \cdot \rangle$ on both sides of the first equation in (10) with $\Theta^{k+1} + \Theta^k$, we have

$$\langle \partial_t \Theta^{k+1}, \Theta^{k+1} + \Theta^k \rangle - 2v \langle \delta_x^2 \Theta^{k+1/2}, \Theta^{k+1/2} \rangle + \frac{h^2}{12} \langle \partial_t [\delta_x^2 \Theta]^{k+1}, \Theta^{k+1} + \Theta^k \rangle = 0 \tag{21}$$

Using Lemma 1 and the boundary approximations $D_{\hat{x}}\Theta_0^k = D_{\hat{x}}\Theta_J^k = 0$, we obtain

$$\|\Theta^{k+1}\|_{L_2}^2 - \|\Theta^k\|_{L_2}^2 + 2\tau v |\|D_x \Theta^{k+1/2}|\|_{L_2}^2 - \frac{h^2}{12}\{|\|D_x \Theta^{k+1}|\|_{L_2}^2 - |\|D_x \Theta^k|\|_{L_2}^2\} = 0$$

By summing from $k = 0$ to $n-1$ we have

$$\|\Theta^n\|_{L_2}^2 - \|\Theta^0\|_{L_2}^2 + 2\tau v \sum_{k=0}^{n-1} |\|D_x \Theta^{k+1/2}|\|_{L_2}^2 - \frac{h^2}{12}\{|\|D_x \Theta^n|\|_{L_2}^2 - |\|D_x \Theta^0|\|_{L_2}^2\} = 0$$

Then we get

$$\begin{aligned} \|\Theta^n\|_{L_2}^2 - \frac{h^2}{12}|\|D_x \Theta^n|\|_{L_2}^2 &\leqslant \|\Theta^0\|_{L_2}^2 - \frac{h^2}{12}|\|D_x \Theta^0|\|_{L_2}^2 \\ &\leqslant \max\left\{\|\Theta^0\|_{L_2}^2, \frac{h^2}{12}|\|D_x \Theta^0|\|_{L_2}^2\right\} \end{aligned}$$

The proof is completed by applying Lemma 2 to the above inequality. □

Remark 5
By taking the inner product $\langle \cdot, \cdot \rangle$ on both sides of the first equation in (10) with $\Theta^{k+1} - \Theta^k$, using Lemma 1 and the boundary approximations $D_{\hat{x}}\Theta_0^k = D_{\hat{x}}\Theta_J^k = 0$, we can obtain

$$\tau \|\partial_t \Theta^{k+1}\|_{L_2}^2 - \frac{h^2 \tau}{12}|\|D_x[\partial_t \Theta^{k+1}]|\|_{L_2}^2 + \frac{v}{2}\{|\|D_x \Theta^{k+1}|\|_{L_2}^2 - |\|D_x \Theta^k|\|_{L_2}^2\} = 0$$

It follows from Lemma 2 that

$$|\|D_x \Theta^{k+1}|\|_{L_2}^2 \leqslant |\|D_x \Theta^k|\|_{L_2}^2$$

Combining this inequality with (20) and using Lemma 3, we obtain the discrete $\|\cdot\|_{L_\infty}$-norm stability

$$\|\Theta^n\|_{L_\infty}^2 \leqslant M_0^2 \|\Theta^n\|_{H^1}^2 \leqslant \frac{3M_0^2}{2}\|\Theta^0\|_{H^1}^2, \quad 1 \leqslant n \leqslant N \tag{22}$$

DOI: 10.1002/fld

Let $e_i^k=\Theta_i^k-\theta_i^k,\ i=-1,0,\ldots,J+1$, where Θ_i^k and θ_i^k are the solutions of (10) and (6), respectively. We then obtain the following error equations:

$$\tfrac{1}{12}(\partial_t e_{i-1}^{k+1}+10\partial_t e_i^{k+1}+\partial_t e_{i+1}^{k+1})-\nu\delta_x^2 e_i^{k+1/2}=R_i^k,\quad 0\leqslant i\leqslant J \tag{23}$$

$$D_{\hat{x}}e_0^k=R_l^k,\quad D_{\hat{x}}e_J^k=R_r^k,\quad e_i^0=0 \tag{24}$$

where R_i^k, R_l^k, and R_r^k denote the truncation errors.

Theorem 6
Assume that the solution of problem (6) is sufficiently smooth. Then there exists a constant $M>0$ such that

$$\max_{1\leqslant n\leqslant N}\|e^n\|_{L_2}^2\leqslant M\max_{0\leqslant k\leqslant n}\{\|R^k\|_{L_2}^2+|R_l^k|^2+|R_r^k|^2\}+\ Mh^4\max_{1\leqslant k\leqslant n}\{|\partial_t R_l^k|^2+|\partial_t R_r^k|^2\} \tag{25}$$

Proof
By taking the inner product $\langle\cdot,\cdot\rangle$ on both sides of (23) with $e^{k+1}+e^k$, we obtain

$$\langle\partial_t e^{k+1},e^{k+1}+e^k\rangle-2\nu\langle\delta_x^2 e^{k+1/2},e^{k+1/2}\rangle+\frac{h^2}{12}\langle\partial_t[\delta_x^2 e]^{k+1},e^{k+1}+e^k\rangle=\langle R^k,e^{k+1}+e^k\rangle \tag{26}$$

Using Lemma 1 and the boundary errors in (24), we have

$$\begin{aligned}
&\{\|e^{k+1}\|_{L_2}^2-\|e^k\|_{L_2}^2\}+2\nu\tau|\|D_x e^{k+1/2}|\|_{L_2}^2-\frac{h^2}{12}\{|\|D_x e^{k+1}|\|_{L_2}^2-|\|D_x e^k|\|_{L_2}^2\}\\
&\quad=2\tau\langle R^k,e^{k+1/2}\rangle+2\tau\nu\{R_r^{k+1/2}e_J^{k+1/2}-R_l^{k+1/2}e_0^{k+1/2}\}\\
&\qquad+\frac{\tau h^2}{6}\{[\partial_t R_l^{k+1}]e_0^{k+1/2}-[\partial_t R_r^{k+1}]e_J^{k+1/2}\}\\
&\quad\leqslant\tau\{\|R^k\|_{L_2}^2+\|e^{k+1/2}\|_{L_2}^2\}+2\tau\nu\{|R_l^{k+1/2}\|e_0^{k+1/2}|+|R_r^{k+1/2}\|e_J^{k+1/2}|\}\\
&\qquad+\frac{\tau h^2}{6}\{|\partial_t R_l^{k+1}\|e_0^{k+1/2}|+|\partial_t R_r^{k+1}\|e_J^{k+1/2}|\}
\end{aligned}$$

It follows from Lemma 3 that

$$|e_0^{k+1/2}|\leqslant M_0\{\|e^{k+1/2}\|_{L^2}+|\|D_x e^{k+1/2}|\|_{L_2}\}$$

$$|e_J^{k+1/2}|\leqslant M_0\{\|e^{k+1/2}\|_{L^2}+|\|D_x e^{k+1/2}|\|_{L_2}\}$$

DOI: 10.1002/fld

With the ε-Cauchy inequality ($ab \leqslant (1/4\varepsilon)a^2 + \varepsilon b^2$) we obtain

$$\{\|e^{k+1}\|_{L_2}^2 - \|e^k\|_{L_2}^2\} + 2\nu\tau |\|D_x e^{k+1/2}|\|_{L_2}^2 - \frac{h^2}{12}\{|\|D_x e^{k+1}|\|_{L_2}^2 - |\|D_x e^k|\|_{L_2}^2\}$$
$$\leqslant \tau M_1 \{\|R^k\|_{L_2}^2 + |R_l^{k+1/2}|^2 + |R_r^{k+1/2}|^2 + h^4 |\partial_t R_l^{k+1}|^2 + h^4 |\partial_t R_r^{k+1}|^2\}$$
$$+ \tau M_1 \|e^{k+1/2}\|_{L_2}^2 + 2\nu\tau |\|D_x e^{k+1/2}|\|_{L_2}^2$$

where

$$M_1 = \max\left\{1,\ \left(1 + 2M_0\nu + \frac{M_0}{6}\right),\ (M_0 + 2M_0^2)\nu,\ \frac{M_0}{12} + \frac{M_0^2}{72\nu}\right\}$$

By summing from $k=0$ to $n-1$ and noting $e^0 = 0$, we obtain

$$\left(1 - \frac{M_1\tau}{2}\right)\|e^n\|_{L_2}^2 - \frac{h^2}{12}|\|D_x e^n|\|_{L_2}^2 \leqslant \tau M_1 \sum_{k=1}^{n-1} \|e^k\|_{L_2}^2 + n\tau M_1 \max_{1\leqslant k\leqslant n} \|R^k\|_{L_2}^2$$
$$+ n\tau M_1 \max_{1\leqslant k\leqslant n} \{|R_l^k|^2 + |R_r^k|^2 + h^4 |\partial_t R_l^k|^2 + h^4 |\partial_t R_r^k|^2\}$$

Taking τ sufficiently small, noting that $n\tau \leqslant T$, and applying Lemma 2 and the discrete Gronwall inequality to the above inequality, the result follows immediately. □

Remark 7

By using a similar argument as above and using the discrete Gronwall inequality, we can obtain the following discrete $\|\cdot\|_{L_\infty}$-norm error estimate:

$$\max_{1\leqslant n\leqslant N} \|e^n\|_{L_\infty}^2 \leqslant M \max_{1\leqslant k\leqslant n} \{\|R^k\|_{L_2}^2 + |R_l^k|^2 + |R_r^k|^2 + |\partial_t R_l^k|^2 + |\partial_t R_r^k|^2\}$$
$$+ Mh^4 \max_{1\leqslant k\leqslant n-1} \{|\partial_t^2 R_l^k|^2 + |\partial_t^2 R_r^k|^2\} \tag{27}$$

where $\partial_t^2 R_l^k = (R_l^{k+1} - 2R_l^k + R_l^{k-1})/\tau^2$.

4. NUMERICAL EXPERIMENTS

In this section, we present some numerical examples to test the accuracy of the proposed method and compare the method with some other available numerical methods. The accuracy of the present method will be measured by the discrete L_2- and L_∞-error norms defined in (15) and (16).

4.1. Examples with homogeneous boundary conditions

To demonstrate efficiency and accuracy of the present method, we consider three test examples in this subsection, taken from [6, 8]. Numerical solutions obtained by the present method are compared with the exact solutions and the results given in [6, 8], and [15–18].

DOI: 10.1002/fld

Example 1
We first consider the Burgers Equation (1) with the initial condition

$$u(x,0)=\sin(\pi x),\quad 0<x<1$$

and homogeneous Dirichlet boundary conditions

$$u(0,t)=u(1,t)=0,\quad 0\leqslant t\leqslant T$$

By applying Hopf–Cole transformation, we obtain the initial condition to problem (6) given as

$$\theta(x,0)=\exp(-(2\pi\nu)^{-1}(1-\cos(\pi x))),\quad 0<x<1$$

The exact Fourier solution of Burgers' equation is given by

$$u(x,t)=2\pi\nu\frac{\sum_{n=1}^{\infty}a_n\exp(-n^2\pi^2\nu t)n\sin(n\pi x)}{a_0+\sum_{n=1}^{\infty}a_n\exp(-n^2\pi^2\nu t)\cos(n\pi x)} \tag{28}$$

where the Fourier coefficients are

$$a_0=\int_0^1\exp(-(2\pi\nu)^{-1}(1-\cos(\pi x)))\,\mathrm{d}x$$

$$a_n=2\int_0^1\exp(-(2\pi\nu)^{-1}(1-\cos(\pi x)))\cos(n\pi x)\,\mathrm{d}x\quad\text{for } n=1,2,\ldots$$

In Tables I and II, numerical solutions obtained by the present method at different nodes and times are displayed and compared with the exact and numerical solutions given by other available methods. It can be seen that the accuracy of our method is similar to the fourth-order iterative finite difference method [8]. Errors generated by using different mesh sizes are given in Table III, which shows that the accuracy of the present method is fourth order.

In Figure 1 we draw both numerical (solid line) and exact (dash-dot line) solution curves generated by using different values of $\nu=1$, 0.1 and 0.01, and this figure shows good agreements

Table I. Comparison of numerical and exact solutions of Example 1 at $t=0.1$ for $\nu=1$ with $h=0.1$.

	Numerical				
	$\tau=0.00001$	$\tau=0.0001$			
x	Exact-explicit [6]	GM [16]	IFD [8]	Present	Exact
0.1	0.11048	0.10958	0.10954	0.10954	0.10954
0.2	0.21159	0.20989	0.20980	0.20980	0.20979
0.3	0.29435	0.29199	0.29190	0.29190	0.29190
0.4	0.35080	0.34709	0.34794	0.34793	0.34792
0.5	0.37458	0.37173	0.37159	0.37157	0.37158
0.6	0.36189	0.35920	0.35906	0.35903	0.35905
0.7	0.31231	0.31003	0.30992	0.30989	0.30991
0.8	0.22955	0.22792	0.22783	0.22780	0.22782
0.9	0.12160	0.12071	0.12069	0.12068	0.12069
$\|e\|_{L_2}$				3.923e−6	
$\|e\|_{L_\infty}$				5.638e−6	

DOI: 10.1002/fld

Table II. Comparison of numerical and exact solutions of Example 1 for $v=0.1$ with $h=0.025$ and $\tau=0.001$.

		Numerical				
x	t	Exact-explicit [6]	FEM [15]	IFD [8]	Present	Exact
0.25	0.4	0.30891	0.31429	0.30889	0.30889	0.30889
	0.6	0.24075	0.24373	0.24074	0.24074	0.24074
	0.8	0.19568	0.19758	0.19568	0.19568	0.19568
	1.0	0.16257	0.16391	0.16256	0.16256	0.16256
	3.0	0.02720	0.02743	0.02720	0.02720	0.02720
0.50	0.4	0.56964	0.57636	0.56963	0.56963	0.56963
	0.6	0.44721	0.45169	0.44721	0.44721	0.44721
	0.8	0.35924	0.36245	0.35924	0.35924	0.35924
	1.0	0.29192	0.29437	0.29192	0.29192	0.29192
	3.0	0.04021	0.04057	0.04021	0.04020	0.04021
0.75	0.4	0.62542	0.62592	0.62544	0.62544	0.62544
	0.6	0.48721	0.49034	0.48722	0.48721	0.48721
	0.8	0.37392	0.37713	0.37392	0.37392	0.37392
	1.0	0.28748	0.29016	0.28748	0.28747	0.28747
	3.0	0.02977	0.01334	0.02977	0.02977	0.02977

Table III. Errors and convergence rate of Example 1 for $v=0.1$ at $t=0.5$ with different mesh sizes.

	$h=0.1$	$\tau=0.05$			
Mesh size	τ, h	$\frac{\tau}{4}, \frac{h}{2}$	$\frac{\tau}{16}, \frac{h}{4}$	$\frac{\tau}{64}, \frac{h}{8}$	$\frac{\tau}{256}, \frac{h}{16}$
$\|e\|_{L_2}$	3.520e−4	1.983e−5	1.212e−6	7.538e−8	4.705e−9
Rate		4.1498	4.0319	4.0074	4.0018
$\|e\|_{L_\infty}$	6.103e−4	3.614e−5	2.271e−6	1.414e−7	8.839e−9
Rate		4.0777	3.9922	4.0058	3.9996

of those curves. For $v=0.001$, the infinite Fourier solution fails to converge. Numerical solution curves for this small value of v at different times are given in the bottom right of Figure 1, and the curves show the correct physical behavior.

Example 2

We consider the Burgers Equation (1) with the initial condition

$$u(x,0)=\sin(2\pi x), \quad 0<x<1$$

and boundary conditions

$$u(0,t)=u(1,t)=0, \quad 0\leqslant t\leqslant T$$

The initial condition to problem (6) is

$$\theta(x,0)=\exp(-(4\pi v)^{-1}(1-\cos(2\pi x)))$$

DOI: 10.1002/fld

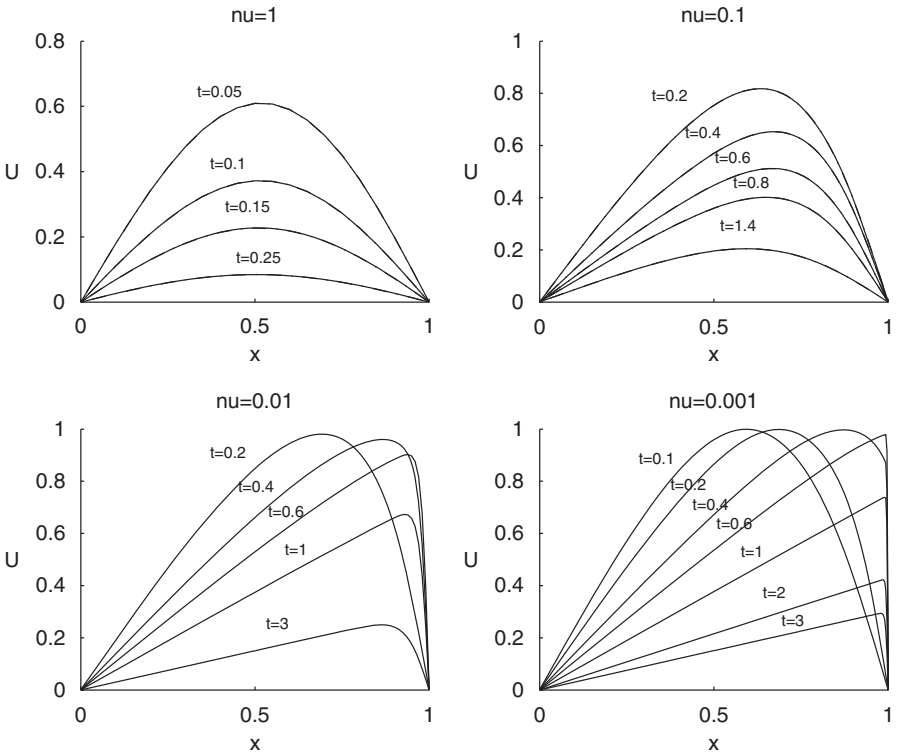

Figure 1. Numerical and exact solutions of Example 1 for different values of v with mesh sizes: $h=0.05$, $\tau=0.0001$ ($v=1$); $h=0.025$, $\tau=0.001$ ($v=0.1$); $h=0.01$, $\tau=0.001$ ($v=0.01$); and $h=0.001$, $\tau=0.001$ ($v=0.001$).

and the exact Fourier solution to Burgers' equation is given by (28). However, in this case, the Fourier coefficients are

$$a_0=\int_0^1 \exp(-(4\pi v)^{-1}(1-\cos(2\pi x)))\,\mathrm{d}x$$

$$a_n=2\int_0^1 \exp(-(4\pi v)^{-1}(1-\cos(2\pi x)))\cos(n\pi x)\mathrm{d}x \quad \text{for } n=1,2,\ldots$$

This example is usually used for simulating the shock formation. The numerical and exact solution curves and distributions of absolute errors for $v=0.005$ are drawn in Figure 2. The curves are not distinguishable due to the closeness of the numerical and exact solutions. One can see from Figure 2 that the maximal absolute errors occur around the critical points. Because the magnitude of differentiations around the critical points is larger than others, the magnitude of truncation errors around these points is larger. Figure 3 shows the numerical solution curves (left) at different times for $v=0.001$ and the numerical solution curves (right) at $t=1.4$ for different values of v. The Fourier solution fails to converge for $v=0.001$. However, the numerical solution curves show the correct physical behavior. We give convergence rate of the present method for Example 2 in Table IV, which shows the fourth-order convergence rate.

DOI: 10.1002/fld

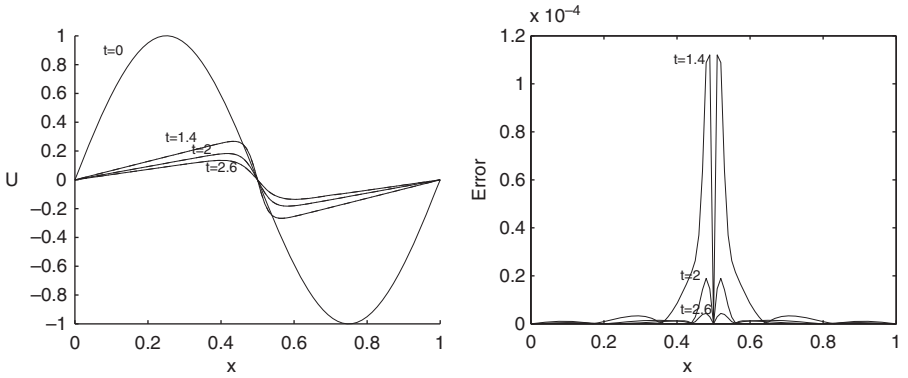

Figure 2. Exact and numerical solutions of Example 2 (left), and distribution of absolute errors (right) for $v=0.005$ with $h=0.01$ and $\tau=0.01$.

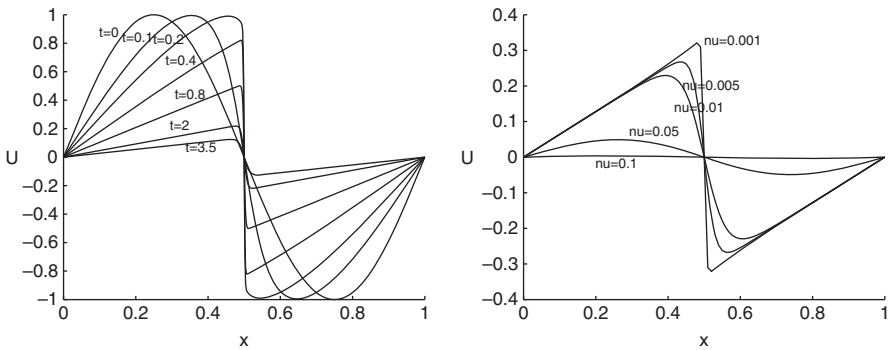

Figure 3. Numerical solutions of Example 2 for $v=0.001$ (left) and numerical solutions at $t=1.4$ for different values of v (right).

Table IV. Errors and convergence rate of Example 2 for $v=0.1$ at $t=0.1$ with different mesh sizes.

	$h=0.1$	$\tau=0.01$				
Mesh size	τ, h	$\frac{\tau}{4}, \frac{h}{2}$	$\frac{\tau}{16}, \frac{h}{4}$	$\frac{\tau}{64}, \frac{h}{8}$	$\frac{\tau}{256}, \frac{h}{16}$	$\frac{\tau}{1024}, \frac{h}{32}$
$\|e\|_{L_2}$	0.0024	1.285e−4	7.673e−6	4.743e−7	2.956e−8	1.846e−9
Rate		4.2229	4.0661	4.0160	4.0040	4.0010
$\|e\|_{L_\infty}$	0.0051	2.573e−4	1.656e−5	1.018e−6	6.350e−8	3.967e−9
Rate		4.3089	3.9576	4.0236	4.0033	4.0005

Example 3

We consider the shock-like solution of the Burgers equation. The analytic solution is given by (cf. [12, 17])

$$u(x,t)=\frac{x/t}{1+\sqrt{t/t_0}\exp(x^2/4vt)}, \quad t\geqslant 1 \tag{29}$$

DOI: 10.1002/fld

where $t_0 = \exp(1/8\nu)$. The initial condition is taken from (29) by setting $t = 1$ and boundary conditions $u(a,t) = u(b,t) = 0$ are used. By the Hopf–Cole transformation, the initial condition to problem (6) is given by

$$\theta(x,1) = \exp\left\{\log\left(\frac{1+\sqrt{1/t_0}\exp(x^2/4\nu)}{1+\sqrt{1/t_0}}\right) - \frac{x^2}{4\nu}\right\}, \quad a < x < b$$

The numerical (solid line) and exact (dash-dot line) solution curves, and distributions of absolute errors for $\nu = 0.005$ and 0.001 are shown in Figures 4 and 5, respectively. The numerical and exact solutions of Example 3 at different times and nodes, and errors are displayed in Table V. To compare accuracy, the errors of the present and some existing methods are given in Table VI, which shows that the present method gives higher accuracy.

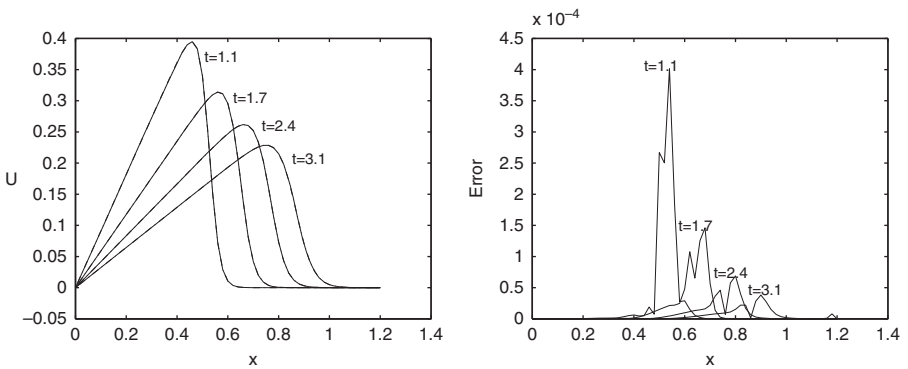

Figure 4. Exact and numerical solutions of Example 3 (left), and distribution of absolute errors (right) for $\nu = 0.005$ with $h = 0.02$ and $\tau = 0.02$.

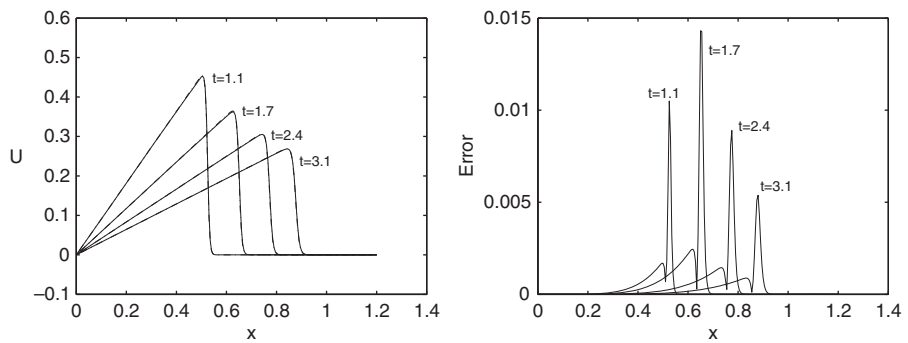

Figure 5. Exact and numerical solutions of Example 3 (left), and distribution of absolute errors (right) for $\nu = 0.001$ with $h = 0.005$ and $\tau = 0.01$.

DOI: 10.1002/fld

Table V. Numerical and exact solutions of Example 3, and errors for $v=0.001$ with $h=0.005$, $\tau=0.01$, and $[a,b]=[0,1.2]$.

	t					
	1.7		2.4		3.1	
x	Numerical	Exact	Numerical	Exact	Numerical	Exact
0.2	0.1176	0.1176	0.0833	0.0833	0.0645	0.0645
0.4	0.2350	0.2353	0.1666	0.1667	0.1290	0.1290
0.6	0.3507	0.3529	0.2495	0.2500	0.1934	0.1935
0.8	0.0000	0.0000	0.0038	0.0033	0.2573	0.2581
1.0	0.0000	0.0000	0.0000	0.0000	0.0000	0.0000
$\|e\|_{L_2}$	0.0018		0.0012		0.00077	
$\|e\|_{L_\infty}$	0.0143		0.0089		0.0054	

Table VI. Comparison of errors for Example 3 with $v=0.005$, $h=0.005$, $\tau=0.01$, and $[a,b]=[0,1]$.

		t		
		1.7	2.5	3.25
Present method	$\|e\|_{L_2}\times 10^3$	0.02018	0.01662	0.96628
	$\|e\|_{L_\infty}\times 10^3$	0.06364	0.09421	6.89958
QRK [18]	$\|e\|_{L_2}\times 10^3$	0.02681	0.03135	1.11149
	$\|e\|_{L_\infty}\times 10^3$	0.09174	0.11515	8.00069
QBC [17]	$\|e\|_{L_2}\times 10^3$	0.07215	0.05103	1.24901
	$\|e\|_{L_\infty}\times 10^3$	0.31153	0.18902	8.98390
CBC [17]	$\|e\|_{L_2}\times 10^3$	2.46642	2.11187	1.92482
	$\|e\|_{L_\infty}\times 10^3$	27.5770	25.1517	21.0489

4.2. Examples with nonhomogeneous boundary conditions

In this subsection, we consider two examples with nonhomogeneous boundary conditions $u(a,t)=u_l(t)$ and $u(b,t)=u_r(t)$. In this case, the linearized problem obtained by the Hopf–Cole transformation is as follows:

$$\theta_t = v\theta_{xx}, \quad a<x<b, \ \ 0<t\leqslant T$$

$$u_l(t)\theta(a,t)+2v\theta_x(a,t)=u_r(t)\theta(b,t)+2v\theta_x(b,t)=0 \tag{30}$$

$$\theta(x,0)=\varphi(x)$$

Then the finite difference scheme for the problem (30) is given by

$$\tfrac{1}{12}(\partial_t\Theta_{i-1}^{k+1}+10\partial_t\Theta_i^{k+1}+\partial_t\Theta_{i+1}^{k+1})-v\delta_x^2\Theta_i^{k+1/2}=0, \quad 1\leqslant i\leqslant J-1$$

$$5\partial_t\Theta_0^{k+1}+\partial_t\Theta_1^{k+1}-\frac{12v}{h}D_x\Theta_0^{k+1/2}+\frac{h}{2v}\partial_t[u_l\Theta_0]^{k+1}-\frac{6}{h}[u_l\Theta_0]^{k+1/2}=0$$

DOI: 10.1002/fld

$$\partial_t \Theta_{J-1}^{k+1} + 5\partial_t \Theta_J^{k+1} + \frac{12v}{h} D_x \Theta_{J-1}^{k+1/2} - \frac{h}{2v} \partial_t [u_r \Theta_J]^{k+1} + \frac{6}{h} [u_r \Theta_J]^{k+1/2} = 0$$

$$\Theta_i^0 = \varphi(x_i)$$

In this case, F_1^k and F_{J-1}^k in (12) should be replaced with $F_1^k - u_l^k$ and $F_{J-1}^k - u_r^k$, respectively.

Example 4

We consider the solution of (1) given by (cf. [8, 19, 20])

$$u(x,t) = \frac{\alpha + \mu + (\mu - \alpha)\exp(\eta)}{1 + \exp(\eta)}, \quad t > 0$$

where $\eta = \alpha(x - \mu t - \beta)/v$, and α, β, and μ are constants. The initial condition is obtained from the exact solution by setting $t = 0$, and the boundary conditions $u(0,t) = 1$ and $u(1,t) = 0.2$ are used. The initial condition to the problem (30) is given by

$$\theta(x,0) = \exp((\alpha - \mu)(x-a)/(2v)) \frac{1 + \exp(\alpha(\beta - x)/v)}{1 + \exp(\alpha(\beta - a)/v)}, \quad t > 1$$

This solution represents a travelling wave, initially situated at $x = \beta$, moving to the right with speed μ. The smaller value of v gives the steeper wave. We simulate the movement of the solution by taking parameters $\alpha = 0.4$, $\mu = 0.6$, and $\beta = 0.125$. The numerical (solid line) and exact (dash-dot line) solution curves, and distributions of absolute errors for $v = 0.01$, 0.005, and 0.001 are drawn in Figures 6, 7, and 8, respectively. These figures show that the agreement between the numerical and exact solutions is satisfactory.

Example 5

As the last example, we consider the one-shock-wave solution of Burgers' equation (1) given by

$$u(x,t) = \frac{\lambda}{2}\left\{1 + \tanh\left[\frac{\lambda}{8v}(-2x + \lambda t)\right]\right\}$$

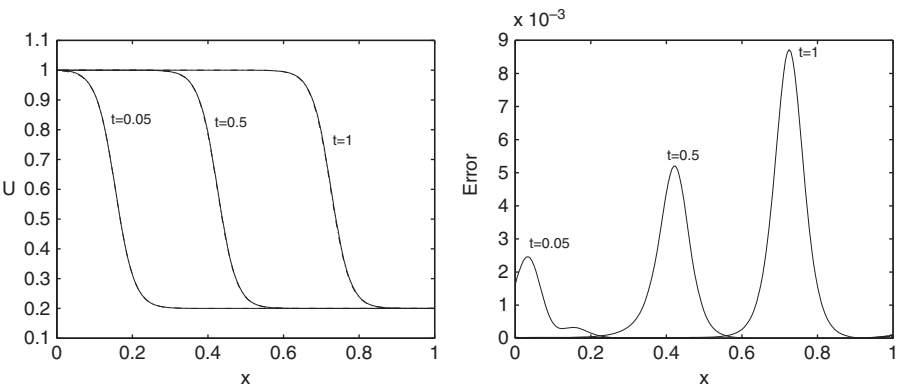

Figure 6. Exact and numerical solutions of Example 4 (left), and distribution of absolute errors (right) for $v = 0.01$ with $h = 0.005$ and $\tau = 0.005$.

DOI: 10.1002/fld

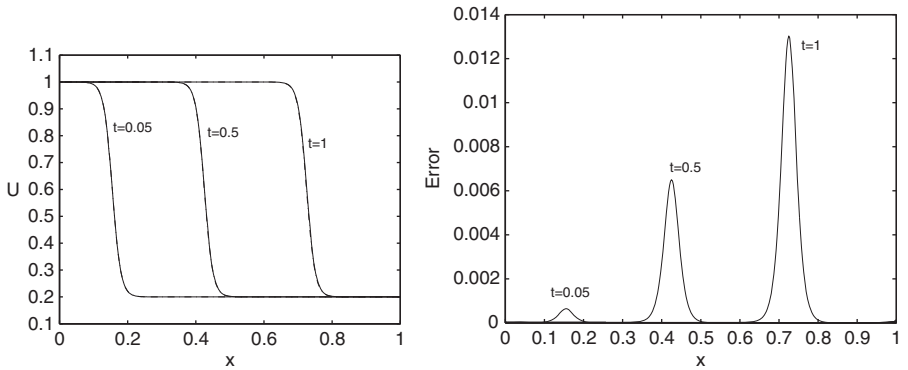

Figure 7. Exact and numerical solutions of Example 4 (left), and distribution of absolute errors (right) for $v=0.005$ with $h=0.0025$ and $\tau=0.0025$.

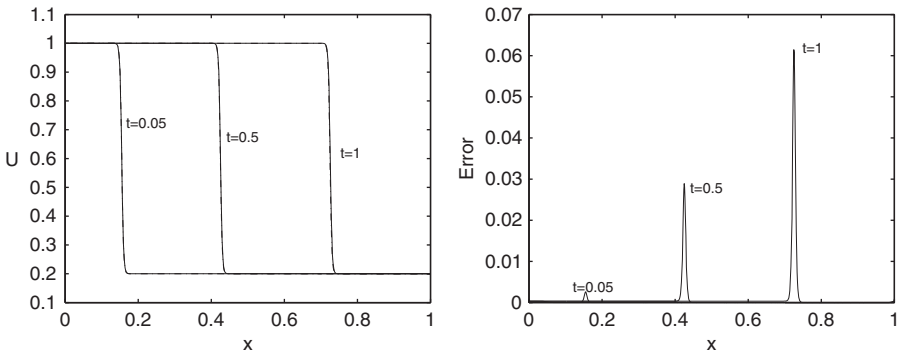

Figure 8. Exact and numerical solutions of Example 4 (left), and distribution of absolute errors (right) for $v=0.001$ with $h=0.001$ and $\tau=0.0005$.

which is the well-known Taylor shock profile [21]. The initial condition to the problem (30) is given by

$$\theta(x,0)=\exp(\alpha(x-a))\frac{\cosh(\alpha x)}{\cosh(\alpha a)}$$

where $\alpha=-\lambda/(4v)$. The numerical experiments are carried out with $\lambda=1.6$. The boundary conditions $u(-5,t)=1.6$ and $u(10,t)=0$ are used. The numerical (solid line) and exact (dash-dot line) solution curves for $v=0.5$ and 0.1 are drawn in Figures 9 and 10, respectively. In these figures, the maximal absolute errors occur at the left boundary and these errors are raised by the finite difference approximations of the nonhomogeneous boundary conditions. One can see that the numerical and exact solutions are in good agreement.

DOI: 10.1002/fld

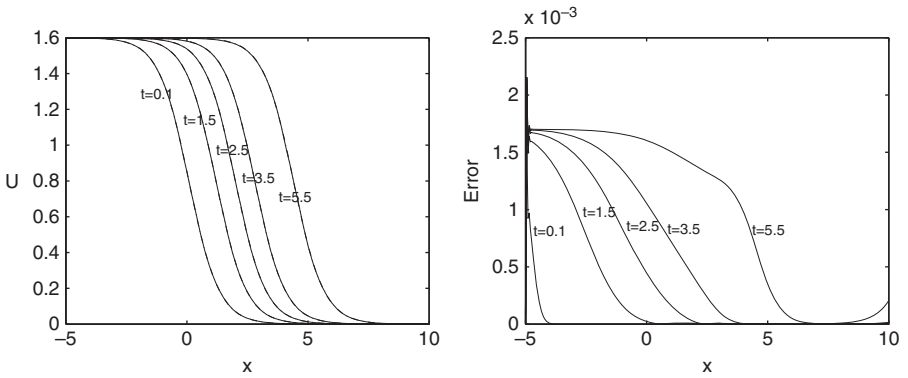

Figure 9. Exact and numerical solutions of Example 5 (left), and distribution of absolute errors (right) for $\nu = 0.5$ with $h = 0.05$ and $\tau = 0.01$.

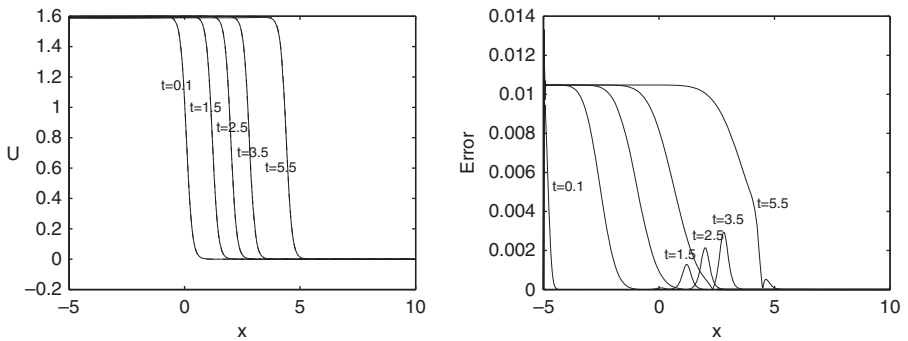

Figure 10. Exact and numerical solutions of Example 5 (left), and distribution of absolute errors (right) for $\nu = 0.1$ with $h = 0.025$ and $\tau = 0.01$.

5. CONCLUSION

A compact finite difference method for one-dimensional Burgers' equation is introduced and analyzed. This method is shown to be unconditionally stable and second- and fourth-order accurate in time and space, respectively. The present method gives a symmetric positive-definite tridiagonal implicit linear system, which can be easily implemented. Our numerical experiments show that the present method offers high accuracy, and they also support the analysis of convergence rate.

ACKNOWLEDGEMENTS

The first author was supported by NNSF of China; 40276008. The last two authors were supported by Changwon National University in 2008.

DOI: 10.1002/fld

REFERENCES

1. Bateman H. Some recent researches on the motion of fluids. *Monthly Weather Review* 1915; **43**:163–170.
2. Burgers JM. A mathematical model illustrating the theory of turbulence. *Advances in Applied Mechanics* 1948; **1**:171–199.
3. Cole JD. On a quasi-linear parabolic equations occurring in aerodynamics. *Quarterly of Applied Mathematics* 1951; **9**:225–236.
4. Benton E, Platzman GW. A table of solutions of the one-dimensional Burgers equations. *Quarterly of Applied Mathematics* 1972; **30**:195–212.
5. Miller EL. Predictor–corrector studies of Burgers' model of turbulent flow. *M.S. Thesis*, University of Delaware, Newark, DE, 1966.
6. Kutluay S, Bahadir AR, Özdes A. Numerical solution of one-dimensional Burgers' equation: explicit and exact-explicit finite difference methods. *Journal of Computational and Applied Mathematics* 1999; **103**:251–261.
7. Kadalbajoo MK, Awasthi A. A numerical method based on Crank–Nicolson scheme for Burgers' equation. *Applied Mathematics and Computation* 2006; **182**:1430–1442.
8. Hassanien IA, Salama AA, Hosham HA. Fourth-order finite difference method for solving Burgers' equation. *Applied Mathematics and Computation* 2005; **170**:781–800.
9. Fletcher CA. A comparison of finite element and difference solutions of the one and two dimensional Burgers' equations. *Journal of Computational Physics* 1983; **51**:159–188.
10. Hon YC, Mao XZ. An efficient numerical scheme for Burgers' equation. *Applied Mathematics and Computation* 1998; **95**:37–50.
11. Kakuda K, Tosaka N. The generalized boundary element approach to Burgers' equation. *International Journal for Numerical Methods in Engineering* 1990; **29**:245–261.
12. Kutluay S, Esen A, Dağ İ. Numerical solutions of the Burgers equation by the least-squares quadratic B-spline finite element method. *Journal of Computational and Applied Mathematics* 2004; **167**:21–33.
13. Mittal RC, Singhal P. Numerical solution of Burgers' equation. *Communications in Numerical Methods in Engineering* 1993; **9**:397–406.
14. Mittal RC, Singhal P. Numerical solution of periodic Burgers' equation. *Indian Journal of Pure and Applied Mathematics* 1996; **27**:689–700.
15. Ozis T, Aksan EN, Özdes A. A finite element approach for solution of Burgers' equation. *Applied Mathematics and Computation* 2003; **139**:417–428.
16. Aksan EN, Özdes A. A numerical solution of Burgers' equation. *Applied Mathematics and Computation* 2004; **156**:395–402.
17. Dağ İ, Irk D, Saka B. A numerical solution of the Burgers equation using cubic B-splines. *Applied Mathematics and Computation* 2005; **163**:199–211.
18. Xie S-S, Heo S, Kim S, Woo G, Yi S. Numerical solution of one-dimensional Burgers' equation using reproducing kernel function. *Journal of Computational and Applied Mathematics* 2008; **214**:417–434.
19. Ali AHA, Gardner GA, Gardner LRT. A collocation solution for Burgers' equation using cubic B-spline finite elements. *Computer Methods in Applied Mechanics and Engineering* 1992; **100**:325–337.
20. Dogan A. A Galerkin finite element approach to Burgers' equation. *Applied Mathematics and Computation* 2004; **157**:331–346.
21. Kraenkel RA, Pereira JG, Manna MA. Nonlinear surface-wave excitations in the Benard–Marangoni system. *Physical Review A* 1992; **46**:4786–4790.

DOI: 10.1002/fld